

Nature of Cyclical Changes in the Timing Residuals from the Pulsar B1642–03

T. V. Shabanova

Pushchino Radio Astronomy Observatory, Astro Space Center, P. N. Lebedev Physical Institute, Russian Academy of Sciences, 142290 Pushchino, Russia

tvsh@prao.ru

ABSTRACT

We report an analysis of timing data for the pulsar B1642–03 (J1645–0317) gathered over the 40-year time span between 1969 and 2008. During this interval, the pulsar experienced eight glitch-like events with a fractional increase in the rotation frequency $\Delta\nu/\nu \sim (0.9 - 2.6) \times 10^{-9}$. We have revealed two important relations in the properties of these peculiar glitches. The first result shows that there is a strong linear correlation between the amplitude of the glitch and the time interval to the next glitch with a slope of about $0.0026 \times 10^{-9} \text{ Hz day}^{-1}$. This relation allows us to predict epochs of new glitches. The second result shows that the amplitude of the glitches is modulated by a periodic large-scale sawtooth-like function. As a result of this modulation, the glitch amplitude varies discretely from glitch to glitch with a step of $1.5 \times 10^{-9} \text{ Hz}$ in the range $(2.4 - 6.9) \times 10^{-9} \text{ Hz}$. The post-glitch time interval also varies discretely with a step of ~ 600 days in the range 900–2700 days. An analysis of the data showed that three modulation schemes with modulation periods of 43 years, 53 years and 60 years are possible. The best model is the 60-year modulation scheme including 12 glitches. We make a conclusion that the nature of the observed cyclical changes in the timing residuals from PSR B1642–03 is a continuous generation of peculiar glitches whose amplitudes are modulated by a periodic large-scale sawtooth-like function. As the modulation function is periodical, the picture of cyclical timing residuals will be exactly repeated in each modulation period or every 60 years.

Subject headings: pulsars: general — pulsars: individual (PSR B1642–03) — stars: neutron — stars: rotation

1. Introduction

The existence of long-term cyclical variations in the spin rate of PSR B1642–03 has been known from the analysis of the first timing data of the pulsar gathered in 1969–1982 (Downs & Reichley 1983; Downs & Krause-Polstorff 1986). During this 13-year interval, the timing residuals of the pulsar exhibited oscillatory but not strictly periodic variations with an amplitude of about 15 ms and a cycle duration of about 1000 days (Cordes & Downs 1985; Cordes 1993). The extension of the observational interval up to 30 years from 1969 to 1999 has shown that the timing residuals have a cyclical behavior during all this interval and the observed variations are characterized by an amplitude varying from 15 to 80 ms and spacing of maxima varying from 1000 to 2600 days (Shabanova et al. 2001). It has been noticed that the observed shape of these cyclical residuals does not depend on the time span of the data analyzed.

The most plausible explanation suggested by the authors (Cordes 1993; Shabanova et al. 2001) was that the long-term cyclical changes in residuals could result from free precession. Free precession due to changes in beam orientation would cause periodic, correlated changes in both the pulse shape and the first frequency derivative. Strictly periodic variations in the pulse profile and pulse arrival times from PSR 1642–03 have not been detected. Nevertheless, robust cyclical behavior in residuals has been interpreted as evidence for slow precession of the neutron star spin axis due to a nonspherical shape of the pulsar. Here we establish that the observed cyclical behavior of the timing residuals from PSR B1642–03 is a result of continuous generation of peculiar glitches whose amplitudes are modulated by some periodic large-scale process.

In this paper, the study of the pulsar’s rotation behavior is based on an analysis of the timing data collected for 40 years at three different observatories. The archival Jet Propulsion Laboratory (JPL) data include the first timing observations of the pulsar B1642–03, which were carried out at 2388 MHz between 1969 and 1982 using antennas of the Deep Space Network of NASA (Downs & Reichley 1983; Downs & Krause-Polstorff 1986). The Jodrell Bank Observatory (JBO) data were obtained at frequencies of 408, 610, 1400, and 1600 MHz over the interval 1981–1999 and taken from the earlier paper (Shabanova et al. 2001). The Pushchino Radio Astronomy Observatory (PRAO) data include the timing data between 1991 and 2008 and a separate observing session in 1984 September–December.

2. Observations and Timing Analysis

Since 1991, the pulsar B1642–03 has been observed at 102 and 112 MHz using the Large Phased Array of the Pushchino Observatory, which is a linearly polarized transit telescope. A 64×20 kHz multi-channel radiometer was used. The resolution of the recorded signals was either 2.56 or 1.28 ms. The duration of each session determined by the width of the antenna beam at the source declination was 3.2 min for the declination of PSR B1642–03. The mean pulse profile in each 20 kHz channel was obtained by synchronous adding of 500 individual pulses with a predicted topocentric pulsar period. After dispersion removal, all the channel profiles were summed to form a mean pulse profile for the given observing session. The topocentric arrival times of the pulses for each observing session were calculated by cross-correlating the mean pulse profile with a standard low-noise template.

The topocentric arrival times collected at JBO, PRAO, and the geocentric arrival times obtained from the archival JPL timing data were all referred to as the barycenter of the solar system at infinite frequency using the program TEMPO ¹ and the JPL DE200 ephemeris. The coordinates of the pulsar that are required for this reduction were taken from Hobbs et al. (2004), together with a proper motion equal to zero (Shabanova et al. 2001).

In order to analyze the variations in the pulsar rotation, a second-order polynomial describing the slow down of the rotational star was fitted to the experimental data. The rotational pulse phase φ at the barycentric arrival times t was calculated as

$$\varphi(t) = \varphi_0 + \nu(t - t_0) + \dot{\nu}(t - t_0)^2/2, \quad (1)$$

where φ_0 , ν , and $\dot{\nu}$ are the pulse phase (measured in cycles), rotation frequency, and first frequency derivative at some reference time t_0 , respectively. The phase residuals, obtained as differences between the observed phase and the phase predicted from a timing model, were used for improving the spin-down parameters of the pulsar. Pulsar parameters ν and $\dot{\nu}$ measured over the 40-year time span of observations are given in Section 3. Residuals derived with these new parameters were used to study variations in the pulsar rotation.

Glitches observed in the rotation frequency of the pulsar B1642–03 are peculiar because their properties differ from those of normal glitches. Usually normal glitches occur as sudden jumps in the pulsar’s rotation frequency, followed by a post-glitch relaxation representing a sum of the decaying $\Delta\nu_d$ and the permanent $\Delta\nu_p$ components (Shemar & Lyne 1996). The large glitches show significant exponential decay which is estimated by the parameter $Q = \Delta\nu_d/(\Delta\nu_d + \Delta\nu_p)$. Normal glitches are characterized by short rise times of less than

¹<http://www.atnf.csiro.au/research/pulsar/tempo>

one day. In contrast, the pulsar B1642–03 exhibits small glitches that have long rise times of about 400–500 days and show significant exponential relaxation ($Q \sim 0.9$) after a glitch.

3. Results

The timing residuals after subtraction of the best-fit spin-down model are presented in Figure 1 over the period from 1969 to 2008. It is seen that timing residuals show clear cyclical behavior over all the 40-year interval. The mean rotation parameters of the pulsar are very stable and are derived with high accuracy over the fit interval MJD 40414–54825: $\nu = 2.579388686097(13)$ Hz, $\dot{\nu} = -11.84578(4) \times 10^{-15} s^{-2}$ at the epoch MJD 40414.1297. The measured value of the second derivative, $\ddot{\nu} \approx 2 \times 10^{-27} s^{-3}$, is mainly determined by an asymmetry of the residual curve with respect to the X -axis over the time span analyzed. So, a corresponding braking index, $n = \nu\ddot{\nu}/\dot{\nu}^2 \sim 30$, may not be related to the secular slowdown of the pulsar’s rotation.

The central part of the residual curve has a one-year gap between 1983 July and 1984 August. The trend of the curve is well traced on this interval, but in order to study variations in the rotation frequency of the pulsar in more detail, this gap needs to be removed. The recovery of the residual curve was based on the method of prediction of the expected pulse arrival times for particular epochs. For the interval, which corresponded to the descending slope of the residual curve between 1983 June and 1986 January, the values of ν , $\dot{\nu}$ were determined by the fitting the timing model. Using the ν , $\dot{\nu}$ obtained and the first point of the indicated interval as a reference point, the expected pulse arrival times were predicted for the epoches spaced by 30 days within the indicated interval. The timing model fitted to all the points of this interval showed that the timing residuals, corresponding to the predicted pulse arrival times, coincided within 1 ms with the residuals, corresponding to the experimental points from the observing session in 1984 September–December and the first points of the 1986 data set.

3.1. The Rotation Behavior of the Pulsar During the Period from 1969 to 2008

Figure 2(a) shows the timing residuals of the pulsar in which the gap in the data observed was removed. Figures 2(b) and 2(c) show the time behavior of the frequency residuals $\Delta\nu$ and frequency derivative $\dot{\nu}$, respectively. The values of ν and $\dot{\nu}$ were calculated from the local fits, performed to arrival time data over intervals of ~ 200 days that overlapped by 100

days. The use of the predicted pulse arrival times allowed us to define rather precisely the epoch and the amplitude of the cycle that were hidden by a gap in the residual curve.

Figure 2(b) shows that the pulsar experienced eight glitch-like events between 1969 and 2008. These events represent peculiar glitches because they are characterized by a slow, almost linear increase in the rotation frequency ν with a long rise time of 400–500 days. All these glitches have a small absolute amplitude observed in the range $\Delta\nu \sim (2.3 - 6.8) \times 10^{-9}$ Hz. This corresponds to the fractional glitch amplitude of $\Delta\nu/\nu \sim (0.9 - 2.6) \times 10^{-9}$. The largest glitch size (glitches 4 and 7) is greater than the smallest one (glitch 1) by a factor of ~ 3 .

All the glitches observed exhibit similar post-glitch behavior. The standard glitch model was not fitted to arrival time data because of the specific properties of the glitches observed. The exponential curve was fitted to the frequency residuals $\Delta\nu$. Figure 2(b) shows that the post-glitch relaxation of glitches 3, 5, and 7 is well described by an exponentially decaying component with a time constant of $\tau \sim 350 - 550$ days. Though the exponential curve is not well fitted to the smaller glitches, it is possible to suppose that all the glitches observed show a significant exponential decay with a large value of $Q \sim 0.9$.

It is clearly seen from Figure 2(c) that the mean value of the frequency derivative $\dot{\nu}$, marked on the plot by the horizontal line, is rather stable over 40 years of observations. Here, as in the case of slow glitches (Shabanova 2007), the increase in the rotation frequency ν during the glitch is accompanied by the decrease in the frequency derivative $\dot{\nu}$. As is seen from this plot, the peaks of $\Delta\dot{\nu}$ across the glitch have an approximately identical magnitude for all the glitches equal to $\Delta\dot{\nu} \approx 0.17 \times 10^{-15} \text{ s}^{-2}$. This makes up $\sim 1.4\%$ of the mean value of $\dot{\nu} \approx -11.84 \times 10^{-15} \text{ s}^{-2}$. The peaks of $\Delta\dot{\nu}$ characterize the steepness of the front in $\Delta\nu$ which practically does not depend on the glitch amplitude.

An analysis of the changes in $\Delta\nu$ showed that the rotation frequency of the pulsar B1642–03 undergoes continuous generation of peculiar glitches. A result of this process is clearly seen in Figure 2(b) – a decrease in $\Delta\nu$ after one glitch at once passes into an increase in $\Delta\nu$ for the next glitch.

3.2. The Relation between the Glitch Amplitude and the Post-Glitch Interval

Figure 3 shows that there is a strong linear correlation between the glitch amplitude and the time interval following the glitch. The two curves indicate that the larger is the glitch amplitude $\Delta\nu_g$, the larger is the relaxation time interval after the glitch ΔT_{rel} and the larger is the time interval to the next glitch ΔT_{max} . We found no evidence of a correlation

between the glitch amplitude and the time interval preceding the glitch.

A linear model was fitted to seven experimental points because the parameters of the last, eighth glitch are not yet known completely. The linear relation obtained between the glitch amplitude $\Delta\nu_g$ and the post-glitch time intervals is described by the expressions:

$$\Delta\nu_g = 0.00261(17) \times \Delta T_{max} - 0.09(0.32), \quad (2)$$

$$\Delta\nu_g = 0.00269(17) \times \Delta T_{rel} + 1.02(0.26), \quad (3)$$

where uncertainties in the parameters are in parentheses and refer to the last digits.

Both the fitted straight lines have a similar slope of about $0.0026(2) \times 10^{-9}$ Hz day⁻¹ and are spaced on the X -axis by 400–500 days, which is a time of a glitch arising. The solid line ΔT_{max} passes through the origin of coordinates. The dotted line ΔT_{rel} indicates the existence of a lower bound for allowed amplitudes. Glitches, having an amplitude less than 1×10^{-9} Hz, should not exist because they will show negative relaxation time.

The linear relation obtained between the glitch amplitude $\Delta\nu_g$ and the post-glitch interval to the next glitch ΔT_{max} allows us to predict epochs of new glitches. In Figure 3, the amplitude of the eighth glitch marked by the asterisk indicates that the interval to the next glitch should be ~ 2000 days. Therefore, the next, ninth glitch will occur around MJD 56300 or in 2013.

The experimental parameters for eight peculiar glitches plotted in Figure 2(b) are given in Table 1. The parameters are shown in the following order: the glitch number; epoch of the point T_{max} , which corresponds to the maximum deviation of $\Delta\nu_{max}$; epoch of the point T_{min} , which corresponds to the minimum deviation of $\Delta\nu_{min}$; the glitch amplitude $\Delta\nu_g = \Delta\nu_{max} + |\Delta\nu_{min}|$; the time interval after the glitch $\Delta T_{rel} = T_{min} - T_{max}$; and the time interval to the next glitch ΔT_{max} . As the eighth glitch still proceeds, some of its parameters are predicted according to relations (2) and (3). These parameters are printed bold.

3.3. The Relation between the Glitch Amplitude and the Glitch Number

Figure 4 shows the relation between the glitch amplitude $\Delta\nu_g$ and the glitch number in the sequence of the glitches observed. It is seen that the first six experimental points, marked by circles around the crosses, make up two rectilinear branches. The fourth glitch has the maximum amplitude. After this glitch, the increase of the glitch amplitude turns into the decrease of the glitch amplitude with the same rate. The ascending branch (points 1, 2, 3, 4) is well described by the straight line $y = ax + b$ with the coefficients $a =$

1.45(0.04), $b = 0.85(0.11)$, and the descending branch (points 4, 5, 6) has the coefficients $a = -1.50(0.35)$, $b = 8.40(0.75)$.

Figure 4 clearly shows that the glitch amplitude is modulated by the sawtooth-like function, both the branches of which have an identical slope of an opposite sign $a = \pm 1.5 \times 10^{-9}$ Hz. As a result of the modulation, the amplitude is changed discretely from glitch to glitch with a step of 1.5×10^{-9} Hz as its magnitude depends on the serial number of the glitch in a given sequence of the glitches. For further calculations, the ascending branch of the modulation function will be approximated by a straight line $y = 1.5x + 0.9$ and the descending branch by a straight line $y = -1.5x + 12.9$, where x is the glitch number 1,2,3, ..., n . The point of intersection of these two lines has the coordinates, $x_0 = 4.0$ and $y_0 = 6.9$, that correspond to the observed parameters of the fourth glitch. Figure 4 shows that the experimental points well agree with the points calculated for these two branches.

According to relations (2) and (3), the discrete changes of the glitch amplitude will cause the discrete changes of the post-glitch intervals (either increase or decrease) with a step of ~ 580 days. The discrete changes of these parameters allow us to estimate more precisely the lower bound of the allowed glitch amplitudes. The first glitch in the given sequence of the glitches has the observed amplitude of 2.3×10^{-9} Hz and is a minimal glitch that can be recorded. A still smaller glitch should have the amplitude of $\sim 0.8 \times 10^{-9}$ Hz, but this glitch cannot exist as it will exhibit a negative relaxation time interval ΔT_{rel} , as it follows from Figure 3. From here, the allowed interval for the glitch amplitudes observed is in the range $(2.4 - 6.9) \times 10^{-9}$ Hz and has the width equal to $A_{max} = 4.5 \times 10^{-9}$ Hz.

As is seen from Figure 4, experimental points 7 and 8 produce the second descending branch of the modulation function that is parallel to the first branch. The derived relation $y = -1.5x + 12.9$ indicates that the predicted amplitudes of these two glitches should be 2.4 and 0.9×10^{-9} Hz, respectively. The comparison of these values with the values observed, indicated in Table 1, shows that the differences between them make up the same value of about $\sim 4.4 \times 10^{-9}$ Hz. This value is very close to the width of the allowed interval for the glitch amplitudes A_{max} . We make a conclusion that the amplitudes observed in glitches 7 and 8 are a result of a forced increase in their initial amplitudes by the value A_{max} . Figure 4 shows that this unusual phenomenon does not exclude and confirms the existence of the modulation process.

The phenomenon of a forced increase in the initial amplitudes of glitches 7 and 8 is also reflected on the timing residuals. Figure 2(a) shows that the pulse arrival times for cycle 7 are earlier as compared with those for cycle 4, though these glitches have a similar shape in Figure 2(b). It looks as if the pulse arrival times kept the information on partial identity of the indicated glitches. At the low frequency of 112 MHz, we found no evidence of any

changes in the shape or intensity of the mean pulse profile among cycles 6, 7, and 8.

3.4. The Modulation Schemes of the Glitch Amplitudes

A study of the peculiar glitches in the rotation frequency of the pulsar B1642–03 has shown that the amplitudes of these glitches are modulated by some periodic large-scale sawtooth-like function. We should define the period and amplitude of this modulation function. The upper bound of modulation is determined by the amplitude of the fourth glitch so this glitch is at a cross point of the ascending and the descending branches of the modulation function. The glitches with the greater amplitude should not be observed. The lower bound of the modulation function is as yet unknown from the observations. An analysis of the data showed that only three modulation schemes that include an even quantity of glitches 8, 10, or 12 are possible. A modulation period cannot include less than eight glitches as this quantity of glitches is already revealed. Note that the ascending and descending branches of the modulation function are formed by the predicted magnitudes of the glitches. The modulation branches, the main and additional, represent sections of this modulation function. They are located in the allowed range and define the observed magnitudes of the glitches.

Scheme 1. A modulation period includes eight glitches as is shown in Figure 5. It means that each rectilinear branch will be formed by the amplitudes of the four glitches. The lower bound of the modulation function will be determined by the predicted amplitude of the eighth glitch because the eighth glitch will lie at a cross point of the descending branch of the first modulation period and the ascending branch of the second modulation period. This glitch is outside of the allowed interval of the glitch amplitudes and has the predicted amplitude of 0.9×10^{-9} Hz. In accordance with this amplitude, the full amplitude of the modulation function will be equal to $\Delta\nu_M = 6 \times 10^{-9}$ Hz. In practice, the observed amplitude of the eighth glitch equals $\sim 5.2 \times 10^{-9}$ Hz and is a result of a forced increase in its initial amplitude by the value A_{max} .

Table 2 lists the predicted glitch parameters for three modulation schemes including 8, 10, and 12 glitches. The predicted parameters for eight glitches observed are given in the upper part of this table. The predicted glitch amplitudes were calculated with the expressions, describing the two branches of the modulation function: the ascending one as $\Delta\nu_g = 1.5x + 0.9$ for $x = 0, 1, 2, 3, 4$ and the descending one as $\Delta\nu_g = -1.5x + 12.9$ for $x = 4, 5, 6, 7, 8$. The duration of the post-glitch time intervals ΔT_{rel} and ΔT_{max} were calculated using relations (2) and (3). The epoch of each glitch T_g was calculated by addition of the epoch of the previous glitch with the corresponding time interval to the next glitch ΔT_{max} . The glitches whose predicted amplitudes $\Delta\nu_g$ are in the forbidden range $-A_{max} =$

$[(+2.4) - (-2.1)] \times 10^{-9}$ Hz will create an additional branch of the modulation function. Their expected observed amplitudes will differ from the predicted one by the value $A_{max} = 4.5 \times 10^{-9}$ Hz. These expected glitch magnitudes together with the corresponding values of ΔT_{rel} and ΔT_{max} are printed bold in parentheses. The predicted parameters for the modulation schemes including 10 and 12 glitches are presented in the middle and lower parts of Table 2, respectively.

Comparison of the predicted parameters, given in Table 2, and the observed parameters, indicated in Table 1, shows that there is a good agreement among the parameters $\Delta\nu_g$, ΔT_{rel} , and ΔT_{max} . The predicted glitch epochs T_g well correspond to the observed glitch epochs T_{max} within the time resolution of ~ 300 days.

As is seen from Figure 5, the ninth glitch will be the first glitch on the ascending branch of the second modulation period. The amplitudes of the next glitches will be absolutely equivalent to the glitch amplitudes of the first modulation period, as their magnitudes depend only on the serial number of the glitch in a given modulation period. By our calculations, the ninth glitch should occur in 2013 (around MJD 56600). If its observed amplitude is equal to $\Delta\nu_g = 2.4 \times 10^{-9}$ Hz, as indicated in Table 2, then the regularity of the given scheme of the modulation will be confirmed. In this case, the duration of the modulation period will be 43 years. This duration is determined by the sum of the post-glitch time intervals ΔT_{max} , indicated in Table 2.

Scheme 2. A modulation period includes 10 glitches as is shown in Figure 6. It is seen that the predicted amplitudes of glitches 8, 9, and 10 are outside of the allowed interval of the glitch amplitudes. Their predicted magnitudes are given in Table 2. The ninth glitch having a negative magnitude will determine the lower bound of the modulation function. In this case, the full amplitude of the modulation will be equal to $\Delta\nu_M = 7.5 \times 10^{-9}$ Hz. The additional branch of the modulation function will include as many as four glitches. The expected observed amplitudes of these glitches will be a result of a forced increase in its initial amplitudes by the value A_{max} and will have the magnitudes that are printed bold in parentheses in the middle part of Table 2. In this scheme, the observed amplitude of the next, ninth glitch of 2013 should be $\Delta\nu_g = 3.9 \times 10^{-9}$ Hz. The duration of the modulation period will be ~ 53 years.

Scheme 3. A modulation period includes 12 glitches as is shown in Figure 7. This modulation scheme looks most preferable because the modulation function is symmetrical in the range $+A_{max}, -A_{max}$. The predicted amplitudes of the first six glitches are in the allowed range $+A_{max} = (6.9-2.4) \times 10^{-9}$ Hz and the predicted amplitudes of the other six glitches are in the forbidden range $-A_{max} = [(+2.4) - (-2.1)] \times 10^{-9}$ Hz. According to relations (2) and (3), the latter glitches cannot exist. Nevertheless, by analogy with the observed glitches 7 and

8, the managing process should transfer the amplitudes of these six glitches to the allowed range by addition of the value A_{max} . Such amplitudes will form the additional branch of the modulation function. Their magnitudes together with the corresponding values of ΔT_{rel} and ΔT_{max} are printed bold in parentheses in the lower part of Table 2. Figure 7 shows that this additional modulation branch will be the mirror image of the main modulation branch. It is clearly seen if we combine point 7 with point 1 and point 10 with point 4.

In this scheme, the lower bound of the modulation function will be determined by the predicted amplitude of the 10th glitch $\Delta\nu_g = -2.1 \times 10^{-9}$ Hz. Then the full amplitude of the modulation function will be equal to $\Delta\nu_M = 9 \times 10^{-9}$ Hz, that is, will be equal to the width of the double interval $2A_{max}$. The expected observed amplitude of the next, ninth glitch of 2013 should be $\Delta\nu_g = 3.9 \times 10^{-9}$ Hz and will be the same as in scheme 2. As is seen from Table 2, these two schemes will differ starting with the 10th glitch that should occur in \sim 2018. The duration of the modulation period in scheme 3 will be about 60 years.

Figure 7 shows that the modulation scheme cannot include more than 12 glitches. All the predicted glitch amplitudes should be inside a double interval $2A_{max}$, otherwise an additional modulation branch cannot be formed of the allowed glitches. Apparently, scheme 3 is the most probable because the modulation function here is symmetrical and its amplitude is equal to the full width of the double interval $2A_{max}$.

4. Discussion

The observed cyclical changes in the timing residuals from PSR B1642–03 is difficult to explain in terms of a free precession model. Strong evidence for a free precession in the pulsar is expected to be the detection of the strictly periodic variations in the timing residuals that should be accompanied by correlated observable changes in the pulse profile shape (Shaham 1977; Nelson et al. 1990; Cordes 1993). A study of the timing behavior of PSR B1828–11 has provided the first evidence of a free precession in the pulsar (Stairs et al. 2000). The authors have revealed long-term, strictly periodic, correlated variations in both the pulse arrival times and the pulse profile and interpreted this phenomenon by precession of a neutron star spin axis.

In the case of PSR B1642–03, no significant changes in the pulse profile were found within our observations at the frequency of 112 MHz. The pulse profile changes were not detected also in the wide frequency range 0.1–1.6 GHz (Shabanova et al. 2001). The absence of observable changes in the pulse profile and the presence of cyclical timing residuals with variable amplitudes and variable interspaces from three to seven years testify that no

significant precession occurs in this pulsar. As discussed above, cyclical timing residuals are a result of continuous generation of peculiar glitches in the pulsar rotation. The finding of the linear relation between the glitch amplitudes and the post-glitch intervals indicates that the timing behavior of this pulsar can be explained well as a glitch phenomenon.

However, note that the timing residuals of the pulsar B1642–03 will exhibit strictly periodic changes but with a very long timescale of about 60 years. As is seen in Figure 7, the glitch amplitudes are modulated by a periodic large-scale sawtooth-like function. The origin of this modulation function is as yet unknown. If the pulse profiles corresponding to the upper and lower parts of this function have different shapes, we could measure the new pulse shape in the nearest 20–30 years.

A study of the relation between the glitch amplitude and the time interval to the next glitch and also to the time interval from the previous glitch was carried out for pulsars that exhibit multiple glitches in the rotation frequency (Wang et al. 2000; Zou et al. 2008). No clear correlation between the size of the glitch and the corresponding inter-glitch intervals has been revealed for any of the research pulsars. The authors supposed that glitches in these pulsars were due to a local phenomenon, which does not depend on global stresses.

The relationship between the size of the glitch and the time interval to the following glitch was revealed only for the 16 ms X-ray pulsar J0537–6910 (Middleditch et al. 2006). During the seven-year period of observations with the *Rossi X-ray Timing Explorer*, this pulsar suffered 21 glitches with a fractional increase in the rotation frequency $\Delta\nu/\nu \sim (0.2 - 6.8) \times 10^{-7}$. Comparison between the glitch parameters for the two pulsars is presented in Figure 8. The data observed for the glitches in J0537–6910 were taken from Table 4 of Middleditch et al. (2006). Note that a characteristic age of the pulsar B1642–03 is $\tau = P/2\dot{P} \sim 3.4 \times 10^6$ years and that of the pulsar J0537–6910 is $\tau \sim 5 \times 10^3$ years.

It is seen that the glitch parameters for these two pulsars are at the different ends of the span of possible magnitudes. The pulsar J0537–6910 shows the largest absolute size of glitches observed in all pulsars $\Delta\nu \sim (1 - 42) \times 10^{-6}$ Hz. In contrast, the absolute size of glitches in B1642–03 is very small, approximately four orders of magnitude smaller. In the pulsar J0537–6910, the time intervals between the glitches vary from 20 to 283 days. In contrast, B1642–03 presents slow processes, the time intervals between the glitches nearly 10 times greater than those seen in J0537–6910 and glitches are peculiar, with a slow, almost linear increase in the rotation frequency during 400–500 days. Nevertheless, both the pulsars exhibit a clear relation between the glitch size and the time interval to the next glitch. Figure 8 shows that the fitted straight line has a slope of about 0.144×10^{-6} Hz day⁻¹ for J0537–6910 (or 6.5 days per μ Hz from Middleditch et al. (2006)) against 0.003×10^{-9} Hz day⁻¹ for B1642–03. The relation between the glitch amplitude and the glitch number for

J0537–6910 is given in Figure 9. It is seen that largest glitch 1 was followed by a series of 20 glitches with the smaller amplitudes. The glitch amplitude has started to oscillate between glitches 5 and 12. However, there is no indication for the existence of a modulation process acting upon the size of the glitches in this pulsar (compare with Figure 4).

Glitches are thought to arise from sudden and irregular transfer of the angular momentum from a more rapidly rotating component of the superfluid interior to the solid crust of a neutron star. In terms of vortex pinning models, the origin of glitches can be explained by the catastrophic unpinning of neutron superfluid vortices from the lattice of nuclei in the inner crust (Anderson & Itoh 1975; Alpar et al. 1984, 1989, 1993; Pines & Alpar 1985). This theory provides a satisfactory explanation for large glitches in pulsars.

The pulsar B1642–03 shows small glitches but the properties of these glitches, such as exponential decay after the glitch and the existence of a linear relation between the glitch amplitudes and the relaxation time intervals, well correspond to the requirements of this theory. In the case of PSR B1642–03, it is necessary to account for the nature of a continuous generation of peculiar glitches and an origin of a modulation process, which forces the glitch amplitudes and the inter-glitch intervals to change with a discrete step. It is also necessary to find out an interpretation of such an unusual phenomenon of the modulation process as the transfer of the amplitudes of the glitches, which are in the forbidden range, to the allowed range by addition of the value A_{max} . We make a conclusion that if the pulsar glitches are due to a variable coupling between the solid crust and the superfluid interior, then in the case of PSR B1642–03 this variable coupling is provided by the predicted and regular events.

5. Summary

An analysis of the timing behavior of PSR B1642–03 over the 40-year data span from 1969 to 2008 has shown that the pulsar rotation frequency is subject to continuous generation of peculiar glitches whose amplitudes are modulated by some periodic large-scale process. We pay attention to two aspects of the phenomenon observed. The first process gives rise to peculiar glitches having similar properties. These glitches are characterized by small amplitudes, long rise times of about 400–500 days, and significant exponential decay ($Q \sim 0.9$) after the glitch. The amplitude of these glitches and the time interval to the following glitch obey a strong linear relation.

The second process modulates the amplitudes of the peculiar glitches in such a manner that their magnitudes depend on the serial number of the glitch in a given modulation period.

As a result of such modulation, the glitch amplitude changes from glitch to glitch with a discrete step of 1.5×10^{-9} Hz in the range $(2.4 - 6.9) \times 10^{-9}$ Hz. This is accompanied by the corresponding changes of the time intervals to the following glitch with a discrete step of ~ 600 days in the range 900–2700 days. We established that the modulation process has a sawtooth character. The most probable amplitude of this modulation may be equal to $\Delta\nu_M = 9 \times 10^{-9}$ Hz and the most probable modulation period may be equal to ~ 60 years.

Besides, the modulation process gives rise to some additional modulation branches that are parallel to the main modulation branches. These branches are composed of the glitches whose predicted amplitudes should be less than the allowed lower limit $\sim 2.4 \times 10^{-9}$ Hz, that is, such glitches should not exist. Nevertheless, these glitches exist, but they have the amplitudes that are a result of a forced increase in the predicted amplitudes by the value A_{max} .

The nature of cyclical changes in the timing residuals from the pulsar B1642–03 lies in a continuous generation of peculiar glitches whose amplitudes are modulated by some periodic large-scale sawtooth-like function. The amplitudes and spacings of the maxima of the cyclical residuals are a reflection of the glitch amplitudes and the post-glitch time intervals in the rotation frequency. The existence of the periodic sawtooth-like modulation of the glitch amplitudes will cause an absolutely identical picture of the timing residuals in each modulation period or every 60 years.

The indicated properties of the peculiar glitches allow us to predict the epochs and the magnitudes of new glitches in the rotation frequency of this pulsar, as is shown in Table 2. PSR B1642–03 is the first glitching pulsar that shows that the pulsar glitches can be the predicted and regular events.

The author thanks R. D. Dagkesamansky for useful discussion and comments, the engineering and technical collective of the PRAO for their aid in carrying out the many-year observations of this pulsar on the LPA antenna. The author is grateful to the referee for helpful comments and suggestions.

REFERENCES

- Alpar, M. A., Anderson, P. W., Pines, D., & Shaham, J. 1984, ApJ, 276, 325
- Alpar, M. A., Chau, H. F., Cheng, K. S., & Pines, D. 1993, ApJ, 409, 345
- Alpar, M. A., Cheng, K. S., & Pines, D. 1989, ApJ, 346, 823

- Anderson, P. W., & Itoh, N. 1975, *Nature*, 256, 25
- Cordes, J. M. 1993, in ASP Conf. Ser. 36, *Planets around Pulsars*, ed. J. A. Phillips, S. E. Thorsett, & S. R. Kulkarni (San Francisco, CA: ASP), 43
- Cordes, J. M., & Downs, G. S. 1985, *ApJS*, 59, 343
- Downs, G. S., & Krause-Polstorff, J. 1986, *ApJS*, 62, 81
- Downs, G. S., & Reichley, P. E. 1983, *ApJS*, 53, 169
- Hobbs, G., Lyne, A. G., Kramer, M., Martin, C. E., & Jordan, C. 2004, *MNRAS*, 353, 1311
- Middleditch, J., Marshall, F. E., Wang, Q. D., Gotthelf, E. V., & Zhang, W. 2006, *ApJ*, 652, 1531
- Nelson, R. W., Finn, L. S., & Wasserman, I. 1990, *ApJ*, 348, 226
- Pines, D., & Alpar, M. A. 1985, *Nature*, 316, 27
- Shabanova, T. V. 2007, *Ap&SS*, 308, 591
- Shabanova, T. V., Lyne, A. G., & Urama, J. O. 2001, *ApJ*, 552, 321
- Shaham, J. 1977, *ApJ*, 214, 251
- Shemar, S. L., & Lyne, A. G. 1996, *MNRAS*, 282, 677
- Stairs, I. H., Lyne, A. G., & Shemar, S. L. 2000, *Nature*, 406, 484
- Wang, N., Manchester, R. N., Pace, R. T., Bailes, M., Kaspi, V. M., Stappers, B. W., & Lyne, A. G. 2000, *MNRAS*, 317, 843
- Zou, W. Z., Wang, N., Manchester, R. N., Urama, J. O., Hobbs, G., Liu, Z. Y., & Yuan, J. P. 2008, *MNRAS*, 384, 1063

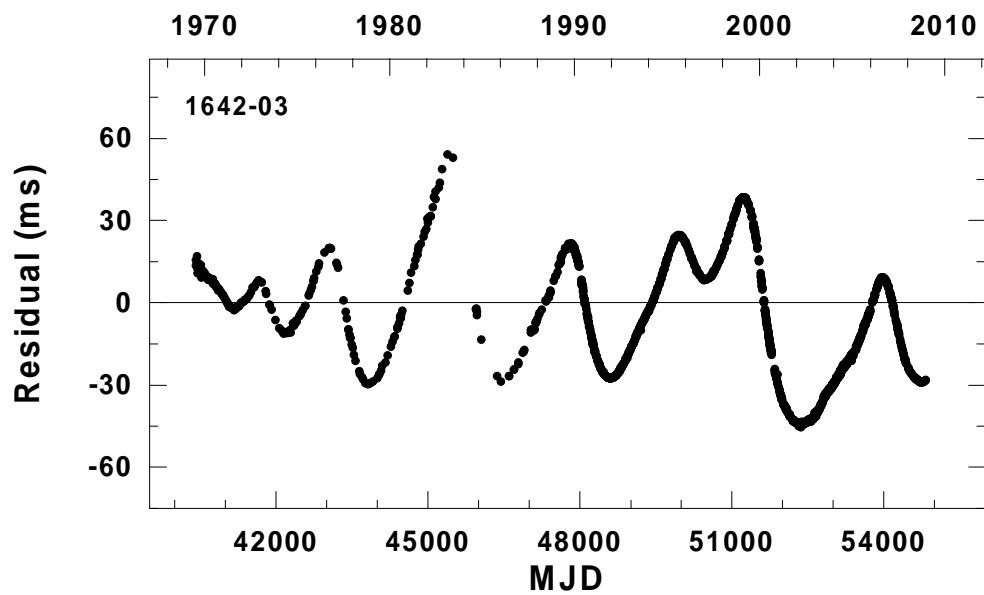


Fig. 1.— Timing residuals from the pulsar B1642–03 over the 40-year time span from 1969 to 2008. The residuals, derived as the observed times minus the predicted ones, are shown after the best fit for ν and $\dot{\nu}$ for all the pulse arrival times. The position was fixed in the fitting procedure. A one-year gap between 1983 and 1984 is seen in the central part of the residual curve.

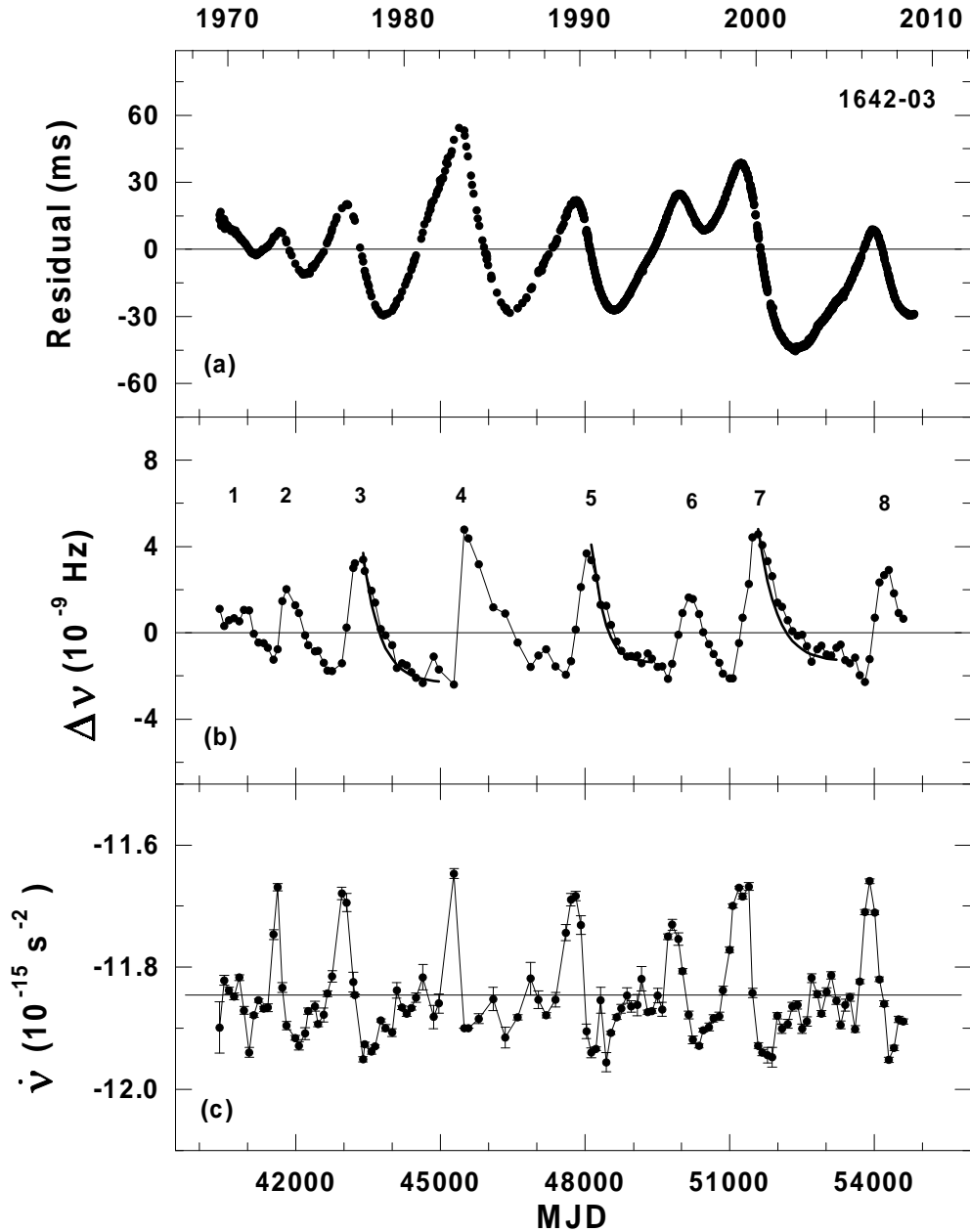


Fig. 2.— Timing behavior of PSR B1642–03 between 1969 and 2008. (a) Residuals are the same as in Figure 1, but the gap in the data between 1983 and 1986 was removed. It has been filled in with points, corresponding to the expected pulse arrival times, predicted by the timing model 1983–1986 for the epochs spaced by 30 days within this gap. (b) The frequency residuals $\Delta\nu$ showing eight peculiar glitches. The bold exponential lines fitted to the post-glitch points for glitches 3, 5, and 7 indicate a significant exponential decay after the glitch with a large value of $Q \sim 0.9$. (c) The changes in the frequency first derivative $\dot{\nu}$ with time. The peaks of $\Delta\dot{\nu}$ characterize the steepness of the front in $\Delta\nu$.

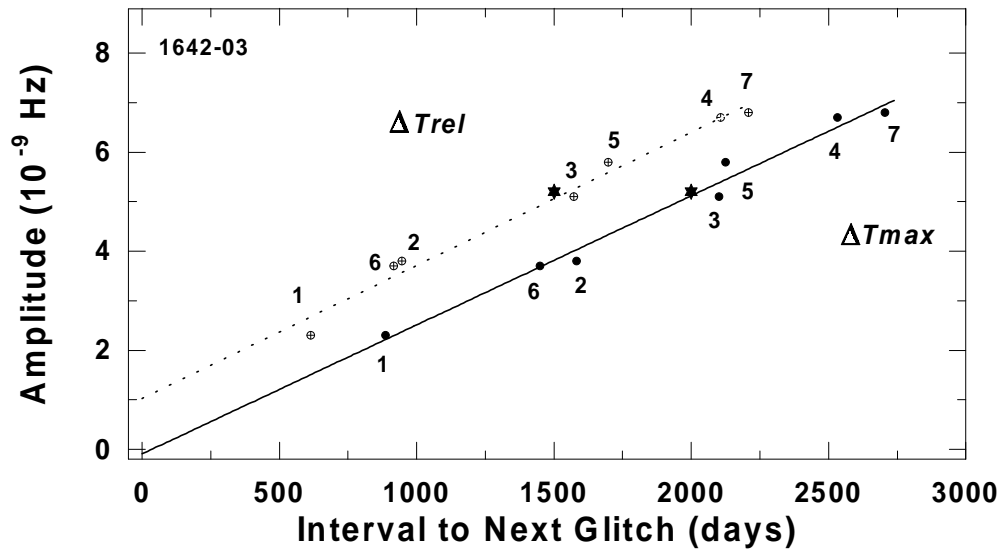


Fig. 3.— Relation between the glitch amplitude and the time interval following the glitch. The dotted line corresponds to the relation between the glitch amplitude and the relaxation time interval ΔT_{rel} (circles around the crosses). The solid line corresponds to the relation between the glitch amplitude and the time interval to the next glitch ΔT_{max} (filled circles). Both the lines have a similar slope of about 0.003×10^{-9} Hz day $^{-1}$. The solid line ΔT_{max} passes through the origin of coordinates. The dotted line ΔT_{rel} indicates the existence of a lower bound for the allowed glitch amplitudes. The amplitude of glitch 8, marked by an asterisk, indicates that the time interval to the next glitch is equal to ~ 2000 days.

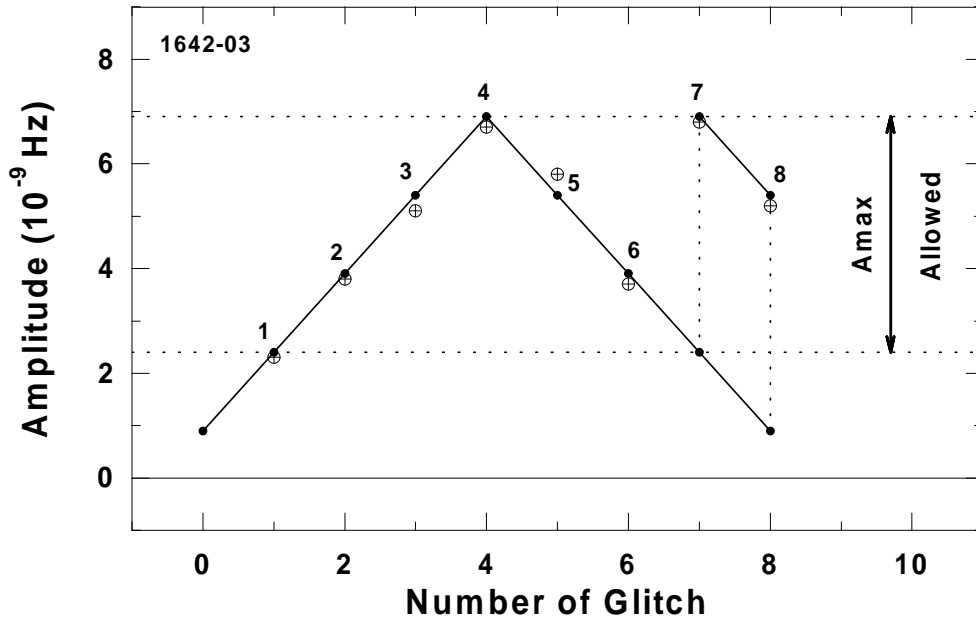


Fig. 4.— Relation between the glitch amplitude and the glitch number. The amplitudes of eight glitches observed are marked by circles around the crosses. The first six points make up the two rectilinear branches which are intersected at point 4. Both the branches have an identical slope of an opposite sign $a = \pm 1.5 \times 10^{-9}$ Hz. The predicted amplitudes of eight glitches observed are marked by filled circles on these two branches. Points 7 and 8 form an additional descending branch, which is parallel to the main descending branch. The displacements of points 7 and 8 from the predicted values on the main branch are marked by the two vertical dotted lines. The two horizontal dotted lines and the arrow A_{max} mark the width of the allowed interval for the observed glitch amplitudes.

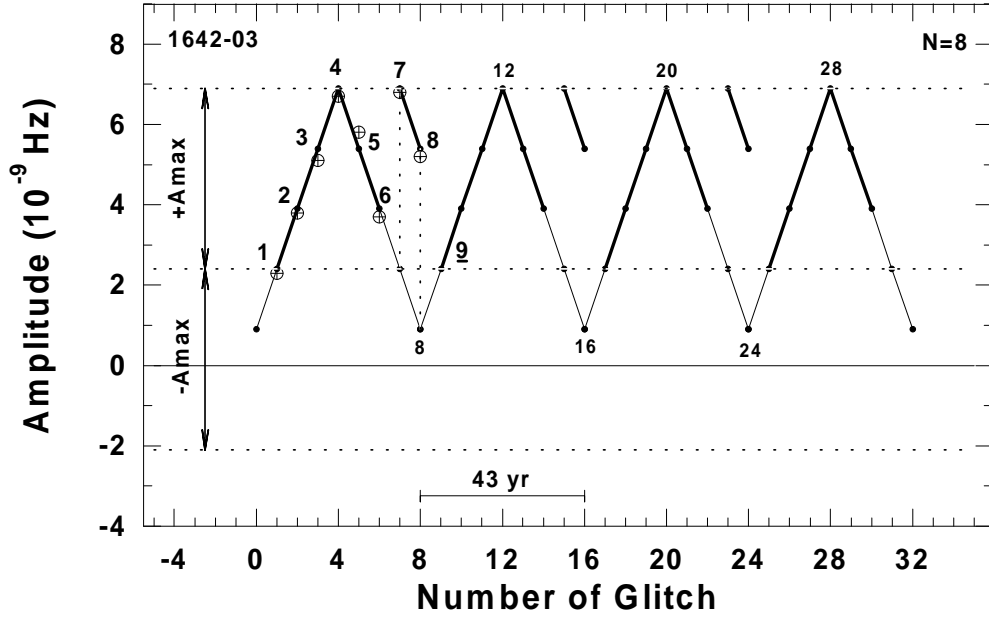


Fig. 5.— Scheme 1 shows four modulation periods, each of which includes eight glitches. The amplitudes of eight glitches observed are marked by circles around the crosses. The three horizontal dotted lines and the two arrows $+A_{max}$ and $-A_{max}$ mark the width of the allowed interval for the observed glitch amplitudes and the width of the forbidden interval, respectively. The predicted points on the ascending and descending branches are marked by filled circles. The two sections of the modulation branches, the main and additional, which define the observed amplitudes of the glitches, are marked by the bold lines in each modulation period. The two vertical dotted lines indicate the displacement of points 7 and 8 from the predicted values on the main descending branch. The full amplitude of the modulation function is equal to $\Delta\nu_M = 6 \times 10^{-9}$ Hz, and the modulation period is equal to 43 years. Glitch 9 of 2013 will be the first glitch on the ascending branch of the second modulation period.

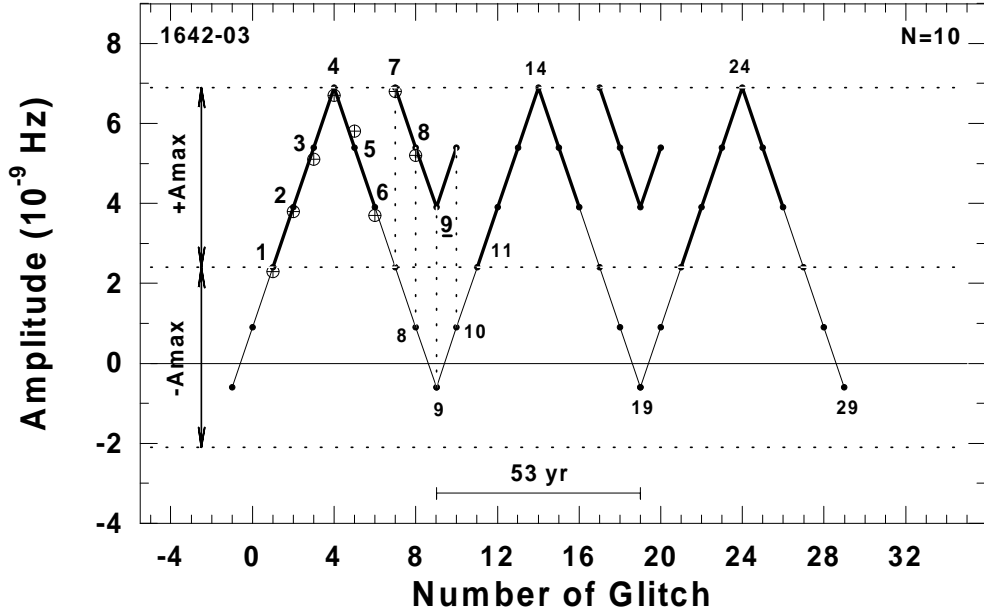


Fig. 6.— Scheme 2 shows three modulation periods, each of which includes 10 glitches. The labels are the same as in Figure 5. The additional modulation branch includes four points 7, 8, 9, and 10. The four vertical dotted lines indicate the displacement of these points from the predicted values on the main branches of the modulation. The amplitude of the modulation is equal to $\Delta\nu_M = 7.5 \times 10^{-9}$ Hz, and the modulation period is equal to 53 years. Point 9 marks the amplitude of the next, ninth glitch of 2013. Glitch 11 of 2023 will be the first glitch on the ascending branch of the second modulation period.

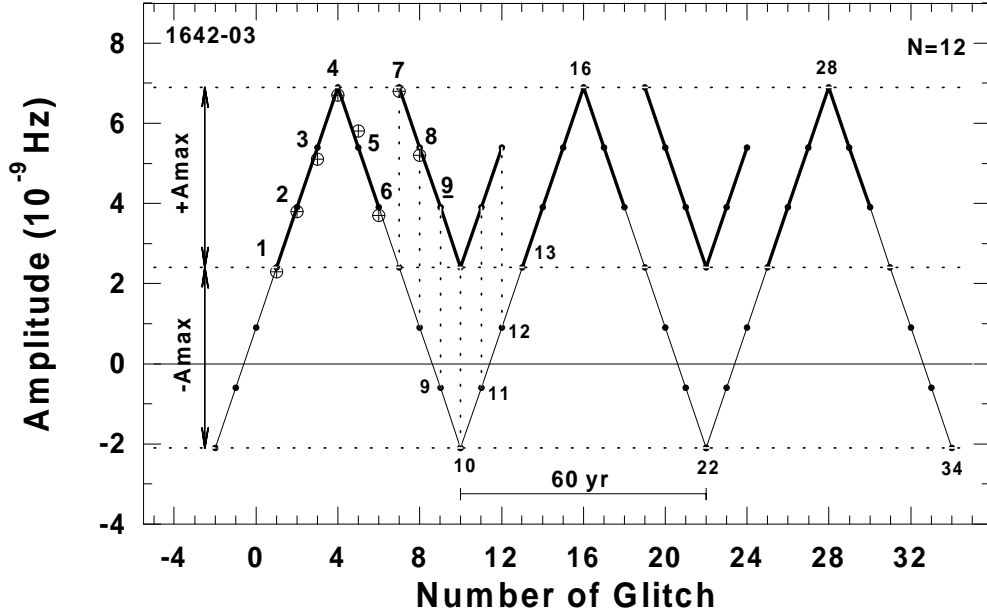


Fig. 7.— Scheme 3 shows three modulation periods, each of which includes 12 glitches. The labels are the same as in Figure 5. The modulation function is symmetrical in the range $+A_{max}$, $-A_{max}$. The two sections of the modulation branches, the main and additional, which are in the allowed range $+A_{max}$, are marked by bold lines in each modulation period. The displacements of six points of the additional branch from the predicted values are marked by six vertical dotted lines. It is seen that the additional modulation branch is the mirror image of the main modulation branch located in the range $+A_{max}$. The full amplitude of the modulation function is equal to $\Delta\nu_M = 9 \times 10^{-9}$ Hz, and the modulation period is equal to ~ 60 years. Point 9 marks the amplitude of the next, ninth glitch of 2013. Glitch 13 of 2030 will be the first glitch on the ascending branch of the second modulation period.

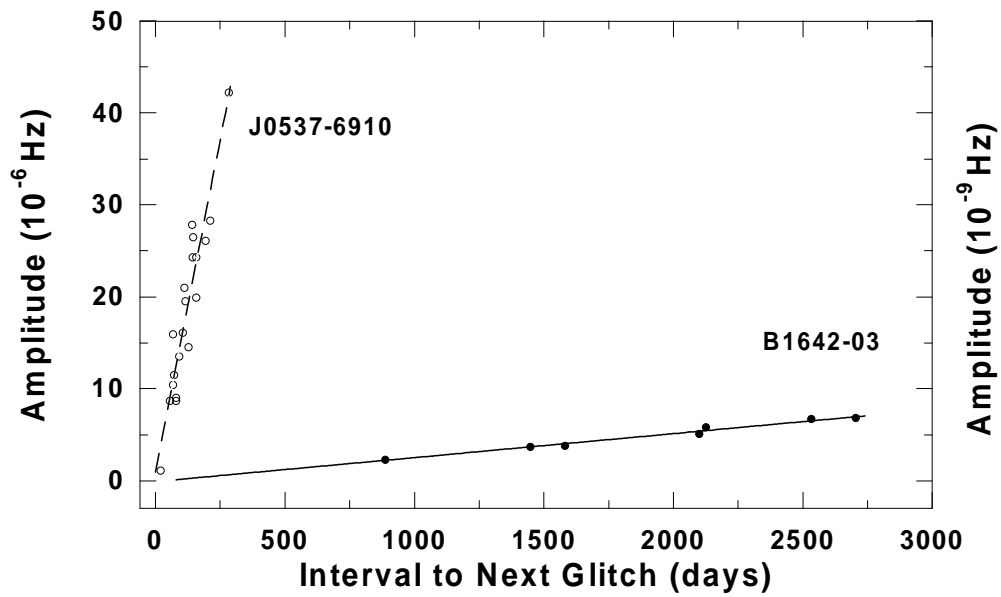


Fig. 8.— Comparison of the two relations showing a correlation between the glitch amplitude and the time interval to the next glitch for the 16 ms X-ray pulsar J0537–6910 and for the pulsar B1642–03. The fitted straight lines have a slope of about $0.144 \times 10^{-6} \text{ Hz day}^{-1}$ for J0537–6910 and a slope of about $0.003 \times 10^{-9} \text{ Hz day}^{-1}$ for B1642–03.

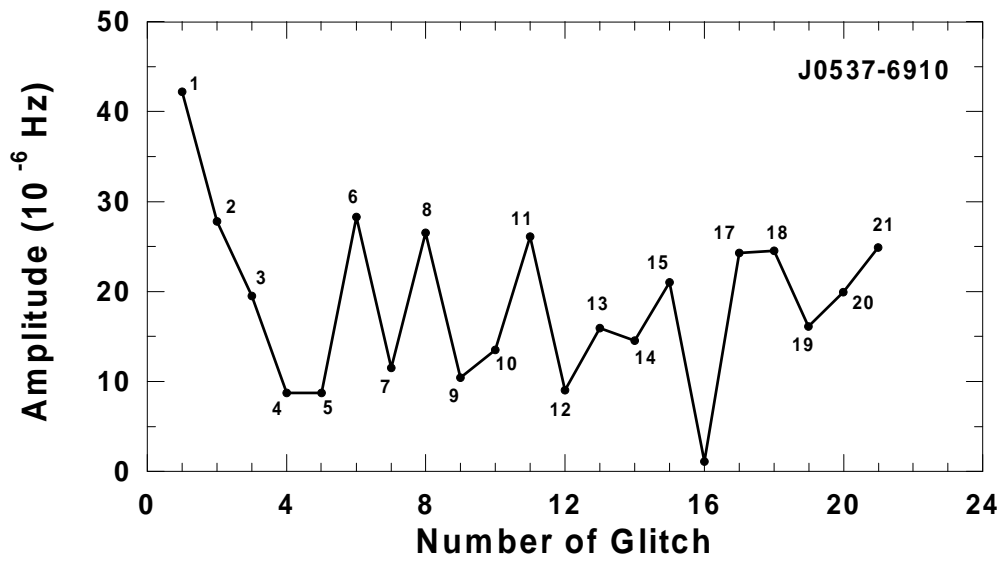


Fig. 9.— Relation between the glitch amplitude and the glitch number for J0537–6910. Largest glitch 1 was followed by a series of 20 glitches with smaller amplitudes. The oscillatory behavior of the glitch amplitudes is clearly visible between glitches 5 and 12. No obvious modulation acting upon the size of the glitches in this pulsar is observed.

Table 1. The Observed Parameters for Eight Peculiar Glitches Revealed in PSR B1642–03 over the 40-year Interval between 1969 and 2008

No.	T_{max} (MJD)	$\Delta\nu_{max}$ (10^{-9} Hz)	T_{min} (MJD)	$\Delta\nu_{min}$ (10^{-9} Hz)	$\Delta\nu_g$ (10^{-9} Hz)	ΔT_{rel} (days)	ΔT_{max} (days)
1	40920	1.0	41534	-1.3	2.3	614	886
2	41806	2.0	42751	-1.8	3.8	945	1582
3	43388	3.4	44959	-1.7	5.1	1571	2101
4	45489	4.8	47596	-1.9	6.7	2107	2532
5	48021	3.7	49719	-2.1	5.8	1698	2126
6	50147	1.6	51062	-2.1	3.7	915	1448
7	51595	4.6	53804	-2.2	6.8	2209	2705
8	54300	2.9	55850	-2.2	5.1	1520	2000

Note. — In column order, the table gives the glitch number; epoch of the point T_{max} , which corresponds to the maximum deviation of $\Delta\nu_{max}$; epoch of the point T_{min} , which corresponds to the minimum deviation of $\Delta\nu_{min}$; the glitch amplitude $\Delta\nu_g = \Delta\nu_{max} + |\Delta\nu_{min}|$; the relaxation time interval after the glitch $\Delta T_{rel} = T_{min} - T_{max}$; and the time interval to the next glitch ΔT_{max} . As glitch 8 still proceeds, some of its parameters are predicted according to relations (2) and (3). They are printed bold.

Table 2. The Predicted Glitch Parameters for Three Modulation Schemes Including 8, 10, and 12 glitches (see Figures 5 – 7, Respectively)

No.	T_g (MJD)	$\Delta\nu_g$ (10^{-9} Hz)	ΔT_{rel} (days)	ΔT_{max} (days)	Date (years)
1	40920	2.4	510	960	1970
2	41880	3.9	1070	1530	1973
3	43410	5.4	1620	2110	1977
4	45520	6.9	2180	2690	1983
5	48210	5.4	1620	2110	1990
6	50320	3.9	1070	1530	1996
7	51850	2.4 (6.9)	510 (2180)	960 (2690)	2000
8	54540	0.9 (5.4)	-40 (1620)	380 (2110)	2008
9	56650	2.4	510	960 scheme 1	2013
8	54540	0.9 (5.4)	-40 (1620)	380 (2110)	2008
9	56650	-0.6 (3.9)	-600 (1070)	-196 (1530)	2013
10	58180	0.9 (5.4)	-40 (1620)	380 (2110)	2018
11	60290	2.4	510	960 scheme 2	2023
8	54540	0.9 (5.4)	-40 (1620)	380 (2110)	2008
9	56650	-0.6 (3.9)	-600 (1070)	-196 (1530)	2013
10	58180	-2.1 (2.4)	-1160 (510)	-773 (960)	2018
11	59140	-0.6 (3.9)	-600 (1070)	-196 (1530)	2020
12	60670	0.9 (5.4)	-40 (1620)	380 (2110)	2024
13	62780	2.4	510	960 scheme 3	2030

Note. — In column order, the table gives the glitch number, the glitch epoch T_g , the glitch amplitude $\Delta\nu_g$, the relaxation time interval after the glitch ΔT_{rel} , the time interval to the next glitch ΔT_{max} , and the glitch date. The amplitudes were calculated as $\Delta\nu_g = 1.5x + 0.9$ for $x = 0, 1, 2, 3, 4$ and as $\Delta\nu_g = -1.5x + 12.9$ for $x = 4, 5, 6, \dots, 10$. The intervals ΔT_{rel} and ΔT_{max} were calculated using relations (2) and (3). The epoch T_g was calculated by addition of the epoch of the previous glitch with the corresponding interval ΔT_{max} . If the predicted $\Delta\nu_g$ was in the forbidden range $-A_{max} = [(+2.4) - (-2.1)] \times 10^{-9}$ Hz, it was increased by the value 4.5×10^{-9}

Hz and was printed bold in parentheses together with its corresponding values of ΔT_{rel} , ΔT_{max} . The first glitch on the ascending branch of the second modulation period was glitch 9 for scheme 1, glitch 11 for scheme 2, and glitch 13 for scheme 3.